Journal of Hazardous Materials 426 (2022) 128134

Contents lists available at ScienceDirect

Journal of Hazardous Materials

journal homepage: www.elsevier.com/locate/jhazmat

Research Paper

Enhanced catalytic peroxymonosulfate activation for sulfonamide antibiotics degradation over the supported CoS_x-CuS_x derived from ZIF-L (Co) immobilized on copper foam

Aofei Du [a], Huifen Fu [a,*], Peng Wang [a,b,c], Chen Zhao [a], Chong-Chen Wang [a,b,c,d,**]

[a] Beijing Key Laboratory of Functional Materials for Building Structure and Environment Remediation, Beijing University of Civil Engineering and Architecture, Beijing 100044, China
[b] Beijing Energy Conservation & Sustainable Urban and Rural Development Provincial and Ministry Co-construction Collaboration Innovation Center, Beijing University of Civil Engineering and Architecture, Beijing 100044, China
[c] Beijing Engineering Research Center of Sustainable Urban Sewage System Construction and Risk Control, Beijing University of Civil Engineering and Architecture, China Beijing University of Civil Engineering and Architecture, Beijing 100044, China
[d] Key Laboratory of Urban Stormwater System and Water Environment (Ministry of Education), Beijing University of Civil Engineering and Architecture, Beijing University of Civil Engineering and Architecture, Beijing 100044, China

HIGHLIGHTS

- Supported CoS_x-CuS_x/CF was synthesized using a self-sacrificing method.
- CF played a vital role in improving the stability and developing of interfacial interaction.
- The regeneration of Co^{2+} by superficial S and Cu^{+} species led to the superior SR-AOP activity.
- CoS_x-CuS_x/CF displayed excellent stability and reusability due to the immobilization of CF.
- A self-developed fixed-bed reactor was used for sulfonamide antibiotics degradation.

GRAPHICAL ABSTRACT

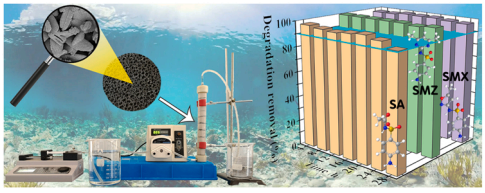

ARTICLE INFO

Editor: Sungjun Bae

Keywords:
Metal-organic framework
Cobalt sulfide
Peroxymonosulfate
Supported catalyst
Sulfonamide antibiotics

ABSTRACT

The CoS_x-CuS_x was firmly immobilized on copper foam (CF) substrate to fabricate supported CoS_x-CuS_x/CF using ZIF-L(Co)/CF as a self-sacrificing template, in which CF substrate played an important role in improving the adhesion between CF and target catalyst as well as the interfacial interaction between CoS_x and CuS_x. The CoS_x-CuS_x/CF performed well in catalytic peroxymonosulfate (PMS) activation, which can accomplish 97.0% sulfamethoxazole (SMX) degradation within 10 min due to the special structure and Co^{2+} regeneration promoted by S^{2-} and Cu^{+}. The influences of pH, PMS dosage, catalyst dosage, co-existing anions and natural organic matter (NOM) on SMX removal were studied in detail. CoS_x-CuS_x/CF presented excellent catalytic activity and reusability, which might be fascinating candidate for real wastewater treatment. The possible pathway of SMX degradation was proposed, and the toxicity of the intermediates during the degradation process were evaluated. It is noteworthy that long-term continuous degradation of sulfonamide antibiotics was achieved using a self-

* Corresponding author.
** Corresponding author at: Beijing Key Laboratory of Functional Materials for Building Structure and Environment Remediation, Beijing University of Civil Engineering and Architecture, Beijing 100044, China.
E-mail addresses: fuhuifen@bucea.edu.cn (H. Fu), wangchongchen@bucea.edu.cn, chongchenwang@126.com (C.-C. Wang).

https://doi.org/10.1016/j.jhazmat.2021.128134
Received 21 October 2021; Received in revised form 16 December 2021; Accepted 20 December 2021
Available online 23 December 2021

developed continuous-flow fixed-bed reactor. This work demonstrated that CF as a substrate to fabricate supported catalysts derived from MOF had great potential in actual wastewater remediation.

1. Introduction

The antibiotics residues as emerging pollutants in wastewater have been widely concerned due to the potential threat to environment and human health. The traditional wastewater treatment technology like activated sludge process is not considered as an ideal method to eliminate antibiotics because of their poor biodegradability. Advanced oxidation processes (AOPs) have received widespread attention due to the high degradation efficiency and nonselective attack on pollutants by generated reactive oxygen species (ROS), especially hydroxyl radical (·OH) and sulfate radical ($SO_4^{\cdot-}$). Compared with Fenton reaction, sulfate radical-based AOPs (SR-AOPs) demonstrated some obvious advantages like the equal or higher redox potential ($SO_4^{\cdot-}$: 2.5–3.1 V *vs.* ·OH: 2.8 V), longer half-life period ($SO_4^{\cdot-}$: 30–40 ms *vs.* ·OH: 20 ns) and more convenient transportation & storage of oxidant (solid peroxysulfate *vs.* liquid H_2O_2) (Chen et al., 2021a,c; Wu et al., 2021).

It was reported that cobalt-based catalysts for SR-AOPs showed a sufficient organic pollutant degradation performance, in which the cobalt sulfides have been widely introduced into SR-AOPs for water purification to improve the catalytic performance via accelerating the regeneration of Co^{2+} by reductive sulfur species. Zhu et al. (2019) found that the cobalt sulfide displayed good peroxymonosulfate (PMS) activation performance to degrade BPA, and the degradation rate exceeded the most reported catalysts by 1–2 orders of magnitude. Li et al. (2020a) demonstrated that the cobalt sulfide as catalyst for SR-AOPs degraded ciprofloxacin (CIP) efficiently at a wide pH range (3−10). As reported, it was deemed that catalysts with porous characteristic would provide abundant active sites to further boost the catalytic activity. Metal-organic frameworks (MOFs) built from metal ions and organic ligands are considered as good self-sacrifice templates to fabricate porous or hollow metal sulfides which exhibited excellent catalytic SR-AOPs degradation activity toward organic pollutants due to their numerous active sites originated from large specific surface area and abundant pore channels (Wu et al., 2020; Fu et al., 2021). Zeolitic imidazolate framework (ZIF), a branch of MOFs, is a novel porous crystalline material integrating the advantages of zeolite and MOFs. ZIF-L, as one kind of typical ZIF, with more active sites owning to its 2D structure attracted considerable attention (Huang et al., 2021a; Peng et al., 2021a,b). Especially, the simple and facile preparation endows ZIF to be a fascinating candidate to construct porous derivatives like metal oxides (Yu et al., 2016, 2020), metal sulfides (Cai et al., 2020) and carbon nanotubes (Ma et al., 2018; Fang et al., 2021). Our group synthesized CoS_x @SiO_2 nanocages derived from ZIF-67(Co) to accomplish superior SR-AOP activity and efficient sulfamethoxazole degradation performance (Wang et al., 2022). However, the powder catalysts are detrimental to the large-scale application due to the difficulty in separating and recycling. It was a hotspot to develop the immobilized/supported catalysts to facilitate the continuous operation. Recently, our group prepared a supported Fe_3O_4 catalyst derived from MIL-88A (Fe) to achieve excellent SR-AOP activity toward the tetracycline hydrochloride degradation (Zhang et al., 2021). As is known to us all, heterojunction is crucial to the improvement of the catalytic activity. However, constructing supported catalysts based on composites is a great challenge because the binding force between catalysts and substrate as well as the interfacial interaction between the individuals should be considered.

Within this work, the supported catalyst CoS_x-CuS_x/CF (CF = copper foam) with heterojunction was fabricated via vulcanizing of ZIF-L(Co)/CF, in which CF acted as both substrate and Cu source. The sulfonamide antibiotics like SMX, sulfacetamide (SA) and sulfamethazine (SMZ) were selected as target pollutants to test the SR-AOP performance of CoS_x-CuS_x/CF. This work aimed to clarify four issues: (i) determining the sulfonamide antibiotics degradation efficiency via SR-AOP with CoS_x-CuS_x/CF as catalyst; (ii) exploring the role of CF on the structure, composition and the SR-AOP activity of CoS_x-CuS_x/CF; (iii) investigating the catalytic mechanism, especially the synergistic effect between CoS_x and CuS_x; (iv) developing a self-developed fixed-bed reactor to achieve the long-term, continuous and efficient sulfonamide antibiotics degradation adopting CoS_x-CuS_x/CF as catalyst.

2. Experimental

2.1. Fabrication of ZIF-L(Co)/CF

A piece of CF (2.0 cm × 2.0 cm) was immersed into a 160 mL aqueous solution containing $Co(NO_3)_2.6H_2O$ (50 mM) and 2-methylimidazole (0.4 M). After 3 h, ZIF-L(Co)/CF was obtained after washed with ultrapure water and dried at 60 ℃ overnight (Scheme 1).

2.2. Synthesis of CoS_x-CuS_x/CF and CuS_x/CF

3.2 mmol thioacetamide (TAA) and 80 mL ethanol (EtOH) along

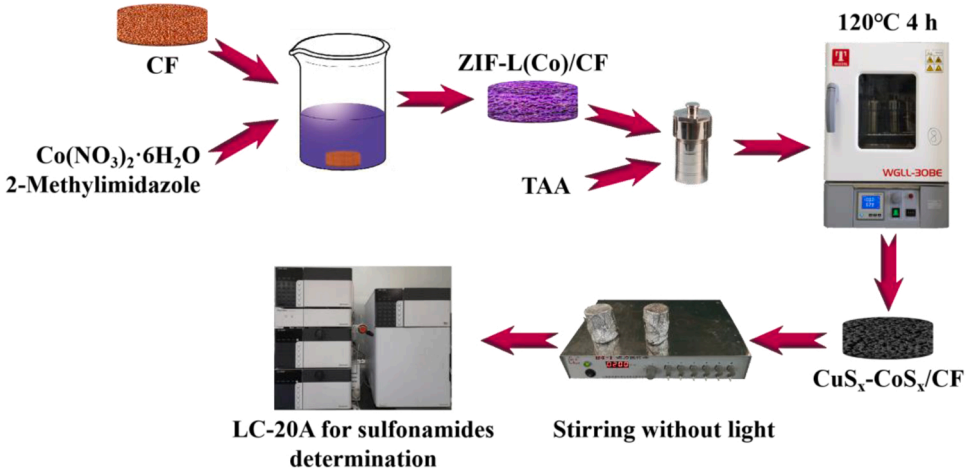

Scheme 1. Synthetic illustration for the preparation of CoS_x-CuS_x/CF and catalytic degradation process of sulfonamide antibiotics.

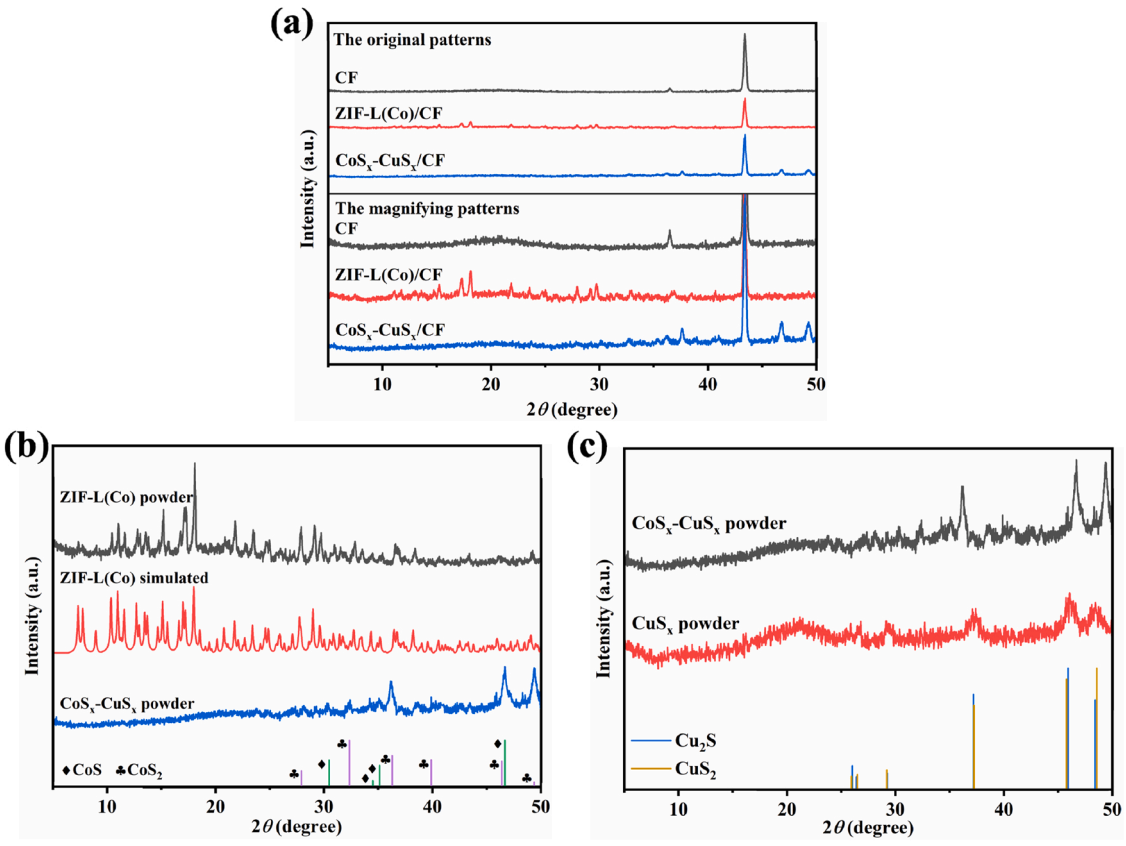

Fig. 1. XRD patterns of different catalysts.

with a piece of as-synthesized ZIF-L(Co)/CF were added into a Teflon-lined autoclave, which was maintained at 120 ℃ for 4 h. The CoS_x-CuS_x/CF was obtained after washed with EtOH and water and dried at 60 ℃ overnight (Scheme 1). The mass loading of CoS_x-CuS_x on CF was weighed at *ca.* 4.5 mg/cm^2. The synthesis procedure of CuS_x/CF is identical to that of the CoS_x-CuS_x/CF except replacing ZIF-L(Co)/CF with pristine CF.

2.3. Catalytic peroxymonosulfate activation for sulfonamide antibiotics degradation over CoS_x-CuS_x/CF

Catalytic degradation experiment was conducted in 50.0 mL aqueous solution of sulfonamide antibiotic (5.0 mg/L) in dark, in which the active CoS_x-CuS_x dosage was 4.5 mg and the pH value was adjusted to 7.0 by HNO_3 or NaOH with proper concentrations. SMX degradation was triggered by adding PMS (0.1 mM), then 1.0 mL aliquot was extracted at designed time intervals, filtered with 0.22 μm PTFE membrane, and immediately quenched with methanol. Finally, the residual SMX concentration was measured by LC (LC-20A, Shimadzu, Japan). The experimental procedure was shown in Scheme 1.

2.4. Quantification of sulfate radical and hydroxyl radicals

The $SO_4^{\cdot-}$ radicals were quantified indirectly by detecting the concentration of *p*-benzoquinone (BQ), generated from the reaction of $SO_4^{\cdot-}$ and *p*-hydroxybenzoic (HBA) (Oh et al., 2017). In brief, 1 × 1 cm^2 CoS_x-CuS_x/CF was quickly added into 50 mL aqueous solution (pH = 9.0) containing a certain amount of HBA and 0.1 mM PMS. Then, 1 mL aliquot was drawn out at designed time intervals, filtered with 0.22 μm PTFE membrane and analyzed by LC to quantitatively determine the concentration of BQ. The molar ratio of PMS:HBA was varied from 1:2–1:6 to ensure that the HBA was excessive.

Dimethyl sulfoxide (DMSO) was used as the probe for the quantification of·OH (Tai et al., 2004). The experimental procedure was similar to the Section 2.5 except that HBA was replaced by DMSO. 2 mL aliquot was drawn out at designed time intervals, and quickly injected into a 2.5 mL buffer solution (31.5% Na_2HPO_4 + 68.5% NaH_2PO_4). Then, 0.2 mL 6 mM 2,4-dinitrophenylhydrazine were added into the aliquot and diluted to 5.0 mL. After being maintained at room temperature for 30 min, the mixture was analyzed by LC (LC-20A, Shimadzu, Japan). The volume fraction of DMSO was varied from 0.2% to 2.0% to ensure that the DMSO was excessive.

2.5. Sulfonamides antibiotics Degradation using a self-developed fixed-bed reactor

A self-developed fixed-bed reactor for wastewater treatment was fabricated, in which 10 pieces of round CoS_x-CuS_x/CF (diameter was 2.7 cm) were fixed with silica sand in a polymethyl methacrylate tube. The hydraulic retention time of sulfonamides through the device was 10 min controlled by peristaltic pump, while the concentration of PMS in the system was adjusted to 0.1 mM by micro-injection pump. 10 mL aliquot was extracted at designed time intervals and filtered with 0.22 μm PTFE membrane. The residual SMX concentration as well as the leaching concentrations of Co and Cu were measured by LC (LC-20A, Shimadzu, Japan) and ICP-OES (ICP-5000, Focused Photonics, China), respectively.

3. Results and discussion

3.1. Materials characterizations

As shown in Fig. 1a, the diffraction peaks of ZIF-L(Co)/CF and CoS_x/CF were not obvious from the original patterns due to the strong peak intensity of CF. To obtain more details from the XRD patterns, the original patterns were magnified locally and some tiny diffraction peaks

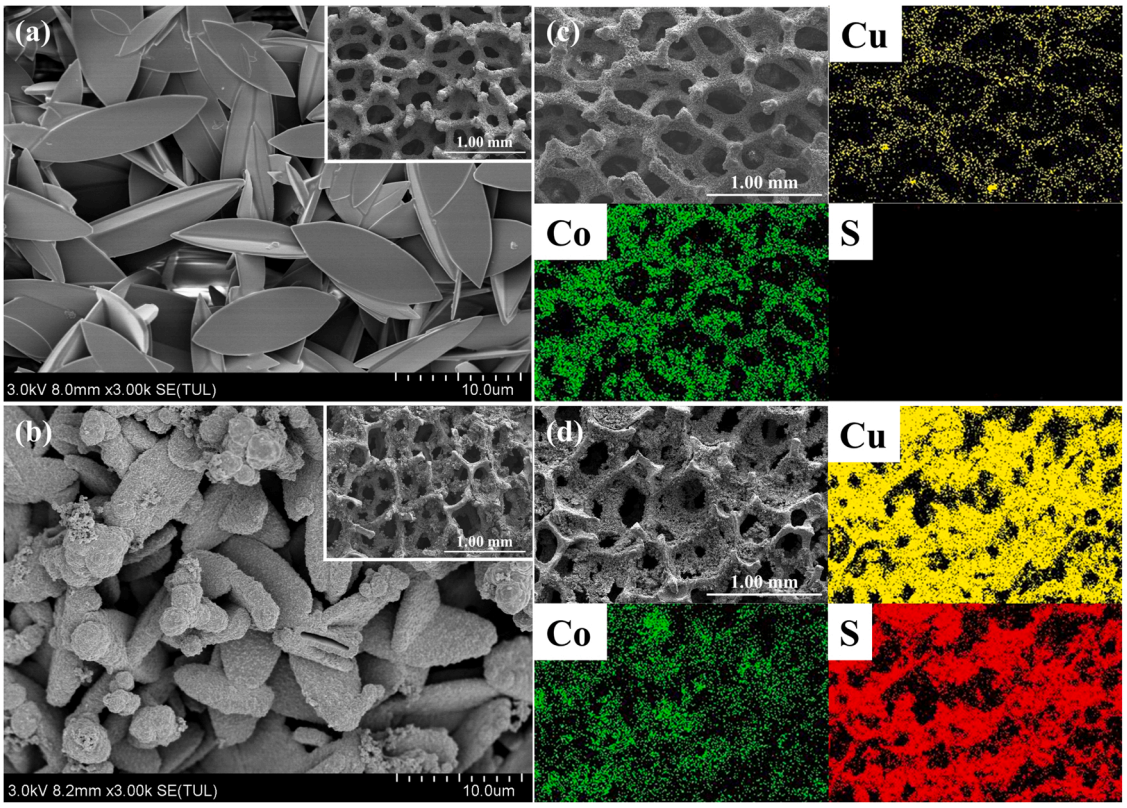

Fig. 2. SEM images of (a) ZIF-L(Co)/CF and (b) CoS_x-CuS_x/CF; Elemental mapping images of (c) ZIF-L(Co)/CF and (d) CoS_x-CuS_x/CF.

were observed which were speculated to be corresponding to ZIF-L(Co) and CoS_x. To verify the attribution of the above tiny peaks, the diffraction patterns of powder sample collected from the sample surface was also conducted (Fig. 1b). The diffraction peaks of ZIF-L(Co) powder and CoS_x powder were same as the above tiny peaks. To be more specific, some characteristic peaks of ZIF-L(Co) powder like 7.3°, 7.7°, 10.3°, 10.9°, 12.7°, 15.2°, 17.0°, 18.0° and 29.0° matched well with the simulated one. The five peaks of CoS_x-CuS_x powder at 30.4°, 34.4°, 35.1°, 46.6° and 54.1° could be obviously observed, which corresponded perfectly with the diffraction plane of (100), (002), (101), (102) and (110) of CoS (ICDD PDF no. 97-062-4842), respectively. Meanwhile, another five peaks of CoS_x-CuS_x powder at 32.3°, 36.2°, 39.8°, 46.3° and 49.3° matched well with the diffraction plane of (200), (210), (211), (220) and (221) of CoS_2 (ICDD PDF no. 97-005-3068), respectively. These results indicated that the CoS_x-CuS_x derived from ZIF-L(Co) mainly consisted of CoS and CoS_2. To prove the formation of CuS_x, the vulcanizing of individual CF substrate was conducted, as shown in Fig. 1c. It is interesting to found that the XRD patterns of both powders collected from CoS_x-CuS_x/CF and CuS_x/CF matched well with Cu_2S (ICDD PDF no. 97-005-3329) and CuS_2 (ICDD PDF no. 97-004-3323). To further confirm the composition of CuS_x, the atomic ratio of Cu and S were measured by EDS (Table S2). The result showed that the ratio of Cu/S was 1.4 which was between 0.5 and 2.0 (atomic ratio of CuS_2 and Cu_2S), further indicating that CuS_x consisted of Cu_2S and CuS_2.

The FTIR spectra of ZIF-L(Co) powder scraped from ZIF-L(Co)/CF was shown in Fig. S1. The characteristic peaks corresponded to the stretching vibration of C=N (1585 cm^{-1}), bending vibration of C-H (1147 cm^{-1}), bending vibration of imidazole ring (around 750 cm^{-1}) and vibration peak of Co-N (423 cm^{-1}), which agreed well with the reported literature (Liu et al., 2017). As for CoS_x-CuS_x powder scraped from CoS_x-CuS_x/CF, the peaks observed at 478 cm^{-1} and 669 cm^{-1} were corresponded to Cu-S bond stretching vibration (Gupta et al., 2021). However, no obvious characteristic peak of CoS_x was observed because characteristic peak of Co-S bond are located in the far infrared region (10–400 cm^{-1}) that beyond the detection region (400–4000 cm^{-1}) of FTIR (Li et al., 2017).

The photographs of the CF, ZIF-L(Co)/CF and CoS_x-CuS_x/CF were provided, as exhibited in Fig. S2. To further observe the microscopic morphology, SEM was used to characterize the supported samples. Fig. 2a-b and Fig. S3 showed that the ZIF-L(Co) on CF exhibited leaf-like shape with an uneven size distribution. It can be seen from Fig. S4a-S4b that the length and width were about 9–17 and 4–6 μm, respectively, according to the analysis results based on SEM images. Vulcanization treatment led to the formation of a hollow structure accompanied with the size shrinkage. As shown in Fig. S4c-S4d, the length and width of the obtained CoS_x-CuS_x supported on CF were mainly distributed at 9–12 μm and 3–6 μm, respectively. Besides, Fig. 2c-d demonstrated the well dispersion of ZIF-L(Co) and CoS_x-CuS_x on CF as Cu, Co and S elements were uniformly distributed on CF. The element Cu was mainly distributed on the framework of the CF in ZIF-L(Co)/CF (Fig. 2c). However, it was observed that the Cu specie migrated into the coated sample to form CuS_x after vulcanization process (Fig. 2d), indicating that CuS_x was produced on the surface of CF, and thus the strong bonding force between CF and the target catalyst was formed. Furthermore, the uniform distribution of Cu, Co and S of CoS_x-CuS_x/CF implied that interfacial interaction between CuS_x and CoS_x was generated, which was beneficial to the electron transfer for the boosted catalytic performance. TEM images of CoS_x-CuS_x powder scraped from the surface of the CoS_x-CuS_x/CF were shown in Fig. S5. Unfortunately, no obvious hollow leaf-like structure was observed, which could be attributed to that strenuous scrape destroyed the morphology of the CoS_x-CuS_x originated from the high binding force of CoS_x-CuS_x on the CF. It is noteworthy that the particles presented in Fig. S5 seems a part of the leaf-like CoS_x-CuS_x originally supported on CF, and the cavity appeared in the middle of the particle. As presented in Fig. S6, the lattice spacing was 0.279 nm, 0.240 nm, 0.287 nm and 0.380 nm, corresponding to the (311) plane of CoS, the (210) plane of CoS_2, the (311) plane of CuS_2 and the (211) plane of Cu_2S, respectively (Yang et al., 2011; Chen et al., 2012; Ji et al., 2022;

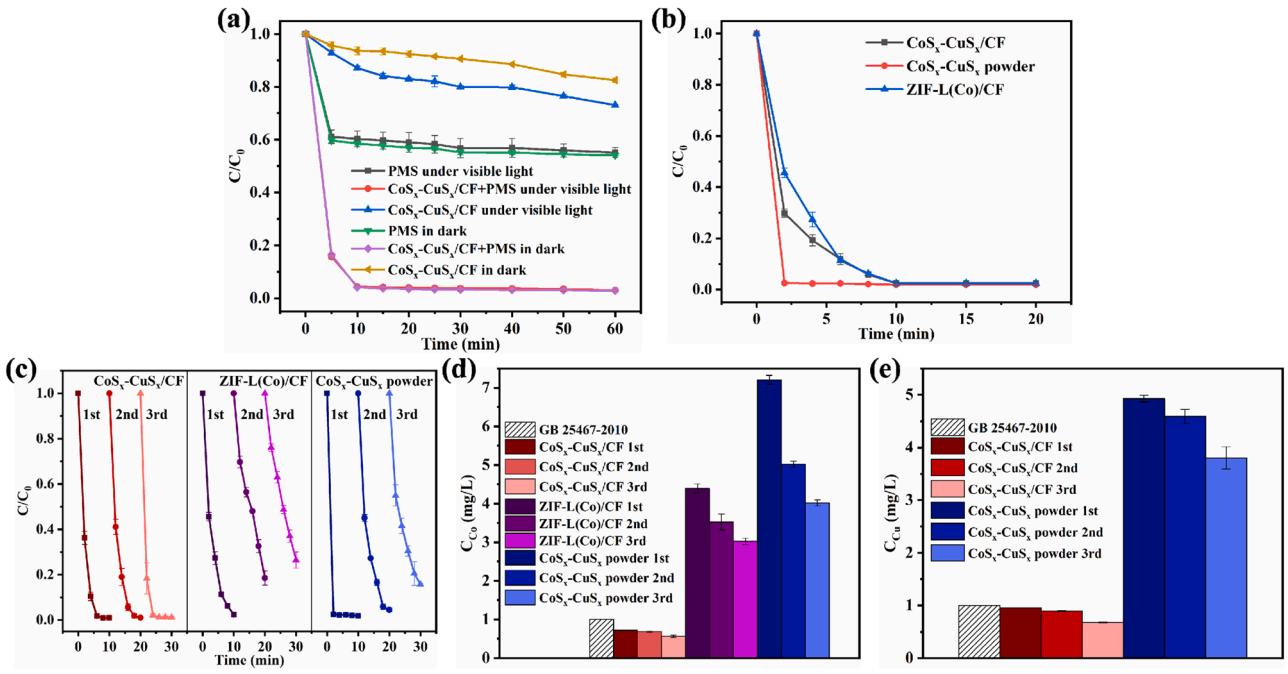

Fig. 3. (a) SMX degradation efficiencies in different conditions; (b) SMX degradation efficiencies and (c) The reusability of CoS_x-CuS_x/CF, ZIF-L(Co)/CF and CoS_x-CuS_x powder; (d) The leaching Co concentrations after each cycle in different system. ($[SMX]_0 = 5$ mg/L, initial pH = 7.0, $[PMS]_0 = 0.1$ mM, $[catalyst]_0 = 90$ mg/L).

Table 1
Summary of SMX degradation efficiencies over various catalysts.

Catalyst/amount (mg/L)	Volume (mL)/ SMX concentration (mg/L)/ PMS dosage (mM)	Operation time (min)	Operation runs	Final degradation efficiency (%)	Ref.
CoS_x-CuS_x/CF/90	50/5/0.1	10	15	97.6	This work
Co_9S_8@N-S-BC/200	60/20/1.6	10	5	100.0	(Wang and Wang, 2020)
CoNC/CNTs/1000	50/25/0.3	45	5	96.4	(Ye et al., 2020)
Fe_3O_4@ZIF-67/100	50/10/0.3	10	5	99.5	(Chen et al., 2021b)
CuO@Al_2O_3/500	300/10/0.4	120	–	99.0	(Yan et al., 2019)
MnO_2/Fe_2O_3/60	80/10/0.8	40	5	90.0	(Guo et al., 2020b)

Yu et al., 2022; He et al., 2020), indicating the formation of heterojunction between CoS_x and CuS_x.

3.2. Catalytic SR-AOP performance

3.2.1. Catalytic peroxymonosulfate activation for SMX degradation

Sulfamethoxazole (SMX), as a kind of common antibiotic, was selected as a model pollutant to test the SR-AOP activity of CoS_x-CuS_x/CF. As showed in Fig. 3a and Fig. S7, the CoS_x-CuS_x/CF-PMS system demonstrated the best SMX degradation activity, in which more than 97.0% degradation efficiency was accomplished within 10 min. The degradation efficiency of SMX were similar under dark and visible light irradiation, indicating that the visible light did not contribute to the SMX degradation. As shown in Fig. S8, the total organic carbon (TOC) removal efficiencies of the CoS_x-CuS_x/CF were 20.3% and 61.0% within 10 min and 120 min, respectively, indicating its good mineralization capacity and potential application in actual wastewater treatment. It can be seen from Table 1 that SMX degradation efficiency of CoS_x-CuS_x/CF was distinctly better than most previously reported catalysts. To further verify the superiority of CoS_x-CuS_x/CF-PMS, SMX degradation efficiencies and stability of CoS_x-CuS_x-PMS, ZIF-L(Co)/CF-PMS and CoS_x-CuS_x/CF-PMS systems were also carried out. As shown in Fig. 3b–e, SMX degradation efficiency, reusability as well as leaching concentrations of Co for CoS_x-CuS_x/CF-PMS system were better than those of the ZIF-L(Co)/CF-PMS system. It was observed that the CoS_x-CuS_x-PMS possessed faster degradation rate than CoS_x-CuS_x/CF-PMS, which resulted from the more exposed active sites of the powder sample. However, the reusability as well as leaching Co and Cu for the CoS_x-CuS_x-PMS was not desired. It is worth noting that the leaching Co and Cu from CoS_x-CuS_x/CF-PMS system were less than the specified value in the corresponding standard like emission standard of industrial pollutants for copper, nickel, cobalt (GB 25467-2010).

3.3. The influences of key parameters on SMX removal by CoS_x-CuS_x/CF-PMS

The initial pH is an important factor in SR-AOPs for organic pollutant degradation (Yi et al., 2021; Zhu et al., 2020). It has been reported that the SMX specifications were influenced by pH as the pK_{a1} and pK_{a2} of SMX are 1.6 and 5.7, respectively, indicating that SMX exists in cationic (SMX^+) at pH < 1.6, neutral (SMX) at 1.6 < pH < 5.7, and anionic form (SMX^-) at 5.7 < pH, respectively (Govindan et al., 2014). However, Fig. 4a showed that CoS_x-CuS_x/CF degraded SMX efficiently in the pH range of 5.0–9.0, and a sharp decline was observed under strong acidic or alkaline condition. As shown in Fig. S9, the Zeta potential of CoS_x-CuS_x/CF was negative in the pH range of 1.0–13.0. It seems that the SMX ionic speciation had negligible influence on SMX degradation. Under the strong acidic condition (pH < 3), excessive protons at low pH would consume $SO_4^{\cdot-}$ and ·OH, resulting in the decrease of SMX degradation (Eqs. 1 and 2) (Yan et al., 2019; Huang et al., 2009). Meanwhile, the

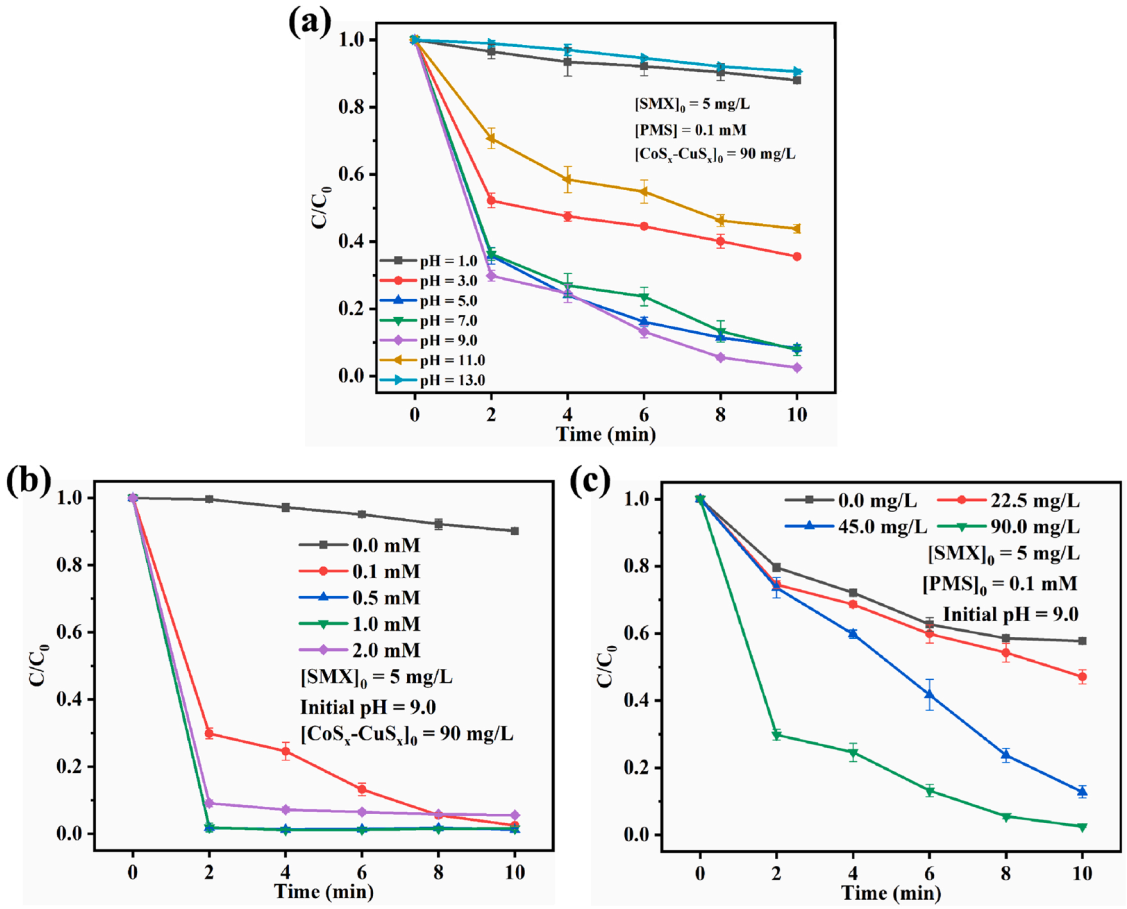

Fig. 4. The influences of (a) initial pH value, (b) PMS dosage and (c) catalyst dosage on SMX degradation efficiencies.

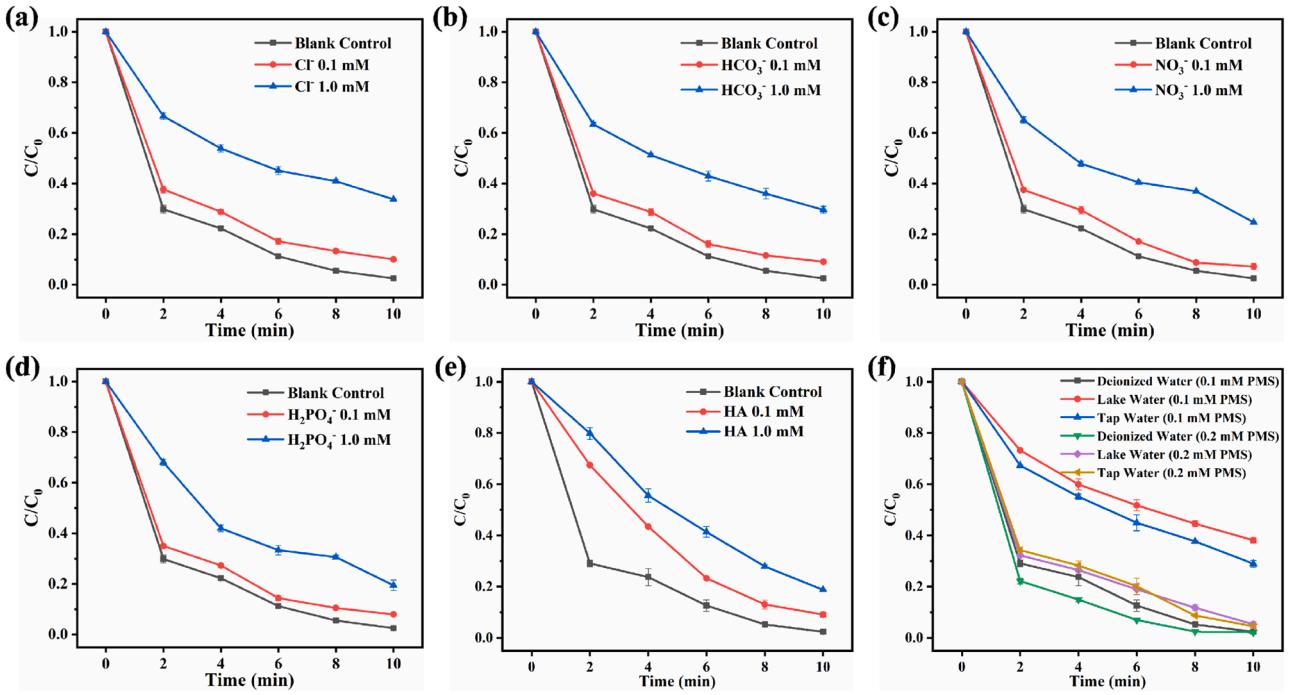

Fig. 5. The influences of Cl^- (a); HCO_3^- (b); NO_3^- (c), $H_2PO_4^-$ (d) and HA (e) on SMX degradation; (f) SMX degradation in simulated wastewater prepared by different water. ($[SMX]_0$ = 5 mg/L, initial pH = 9.0, $[PMS]_0$ = 0.1 or 0.2 mM, $[CoS_x\text{-}CuS_x]_0$ = 90 mg/L).

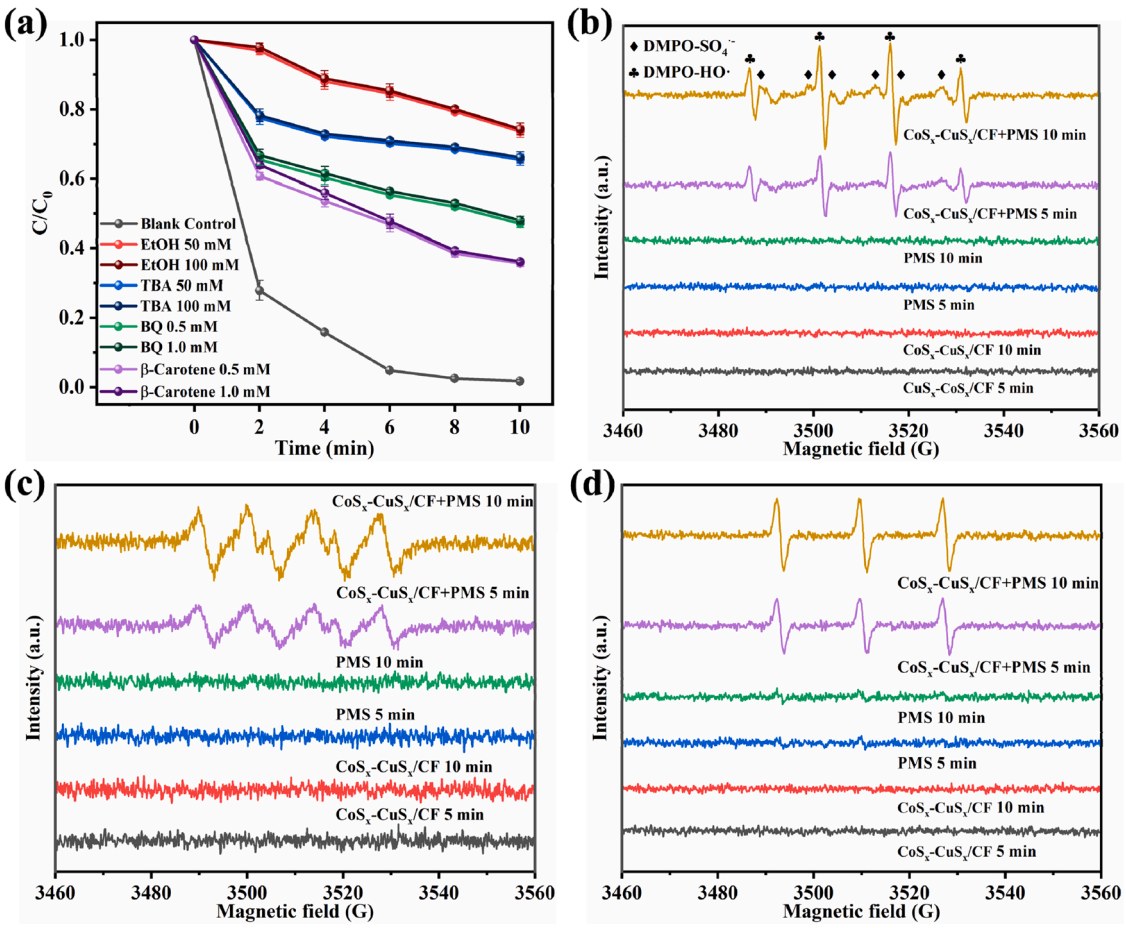

Fig. 6. (a) The influences of different scavengers on SMX degradation in CoS_x-CuS_x/CF-PMS system; The ESR spectra of (b) DMPO-$SO_4^{\cdot-}$, DMPO-·OH, (c) DMPO-$O_2^{\cdot-}$ and (d) TEMP-$^1O_2$ in the CoS_x-CuS_x/CF-PMS system. ($[SMX]_0$ = 5 mg/L, initial pH = 9.0, $[PMS]_0$ = 0.1 mM, $[CoS_x\text{-}CuS_x]_0$ = 90 mg/L).

instability of metal sulfides in strong acidic condition would also be responsible for the decrease of SMX degradation as XRD results suggested that the structure of CoS_x-CuS_x collapsed after catalytic reaction at low pH values like 1.0 and 3.0 (Fig. S10). The dominant species is SO_5^{2-} under strong alkaline condition as the pK_{a2} of PMS is 9.4, which is difficult to be activated to degrade SMX (Huang et al., 2009). Meanwhile, the self-decomposition of PMS in strong alkaline environment could also lead to the decrease of SMX degradation (Chen et al., 2016).

$$\cdot OH + H^+ + e^- \rightarrow H_2O \quad (1)$$

$$SO_4^{\cdot-} + H^+ + e^- \rightarrow HSO_4^- \quad (2)$$

PMS concentration is also a parameter to influence the SMX degradation (Wang et al., 2022). As shown in Fig. 4b, with the increase of PMS concentration, SMX degradation efficiency firstly increased, then decreased, and reached the highest when the PMS concentration was 0.5 mM. PMS concentration was positively correlated to the yield efficiency of ROS to some extent, so that the increase of PMS concentration facilitated the removal of SMX. In our case, the SMX degradation efficiencies were improved when the PMS concentration increased from 0 to 0.5 mM. However, the decline of SMX degradation was observed with further increasing the PMS concentration to 2.0 mM, which was attributed to the self-quenching of free radicals (Cao et al., 2019). In addition, the excessive PMS would react with ROS like·OH and $SO_4^{\cdot-}$ to produce weaker radical $SO_5^{\cdot-}$ (Guan et al., 2011), leading to the decreasing SMX degradation. Also, the increase of SMX degradation efficiency was not obvious when the PMS concentration is larger than 0.1 mM. In order to make full use of PMS, the optimal PMS concentration was selected as 0.1 mM. The influence of catalyst dosage (0–90 mg/L CoS_x-CuS_x) on SMX degradation by PMS activation was also explored. As shown in Fig. 4c, the SMX degradation efficiencies gradually increased with the increase of CoS_x-CuS_x dosage, resulting from the more exposed active sites.

3.4. Effects of co-existing anions and NOM

Some common anions like Cl^-, HCO_3^-, NO_3^- and $H_2PO_4^-$ may influence SMX degradation behaviors during the SR-AOP process by quenching free radicals to generate new weaker active substances or being adsorbed on the catalyst surface (Qi et al., 2014; Ren et al., 2020). As illustrated in Fig. 5a, the SMX degradation efficiencies decreased from 97.6% to 90.0% and 66.2% in the presence of 0.1 and 1.0 mM Cl^-, respectively, which could be attributed to the generation of less reactive chlorine species like Cl·, $Cl_2^{\cdot-}$ and ClOH. On the one hand, PMS could oxidize Cl^- to produce weaker active Cl_2, which consumed PMS (Eq. 3) (Ao and Liu, 2017). On the other hand, Cl^- could react with the generated ROS to produce other less reactive chlorine species (Eqs. 4–9) (Govindan et al., 2014; Zhou et al., 2016; Wang et al., 2017). When HCO_3^- presented in the system, SMX degradation efficiencies decreased from 97.6% to 90.8% (0.1 mM HCO_3^-) and 70.4% (1.0 mM HCO_3^-), as shown in Fig. 5b. There was a balance process between HCO_3^- and CO_3^{2-}, in which the CO_3^{2-} could quench $SO_4^{\cdot-}$ and·OH (Eqs. 10–12) (Neta et al., 1988), leading to the decline of SMX degradation. Fig. 5c showed that SMX degradation efficiency decreased from 97.6% to 92.8% and 75.4% with the addition of 0.1 and 1 mM NO_3^-, respectively. NO_3^- could also react with the generated ROS to form weaker NO_3·(Eqs. 13–14) (Neta et al., 1988), which was detrimental to the removal of SMX. When the system contained $H_2PO_4^-$ (Fig. 5d), the SMX degradation efficiency

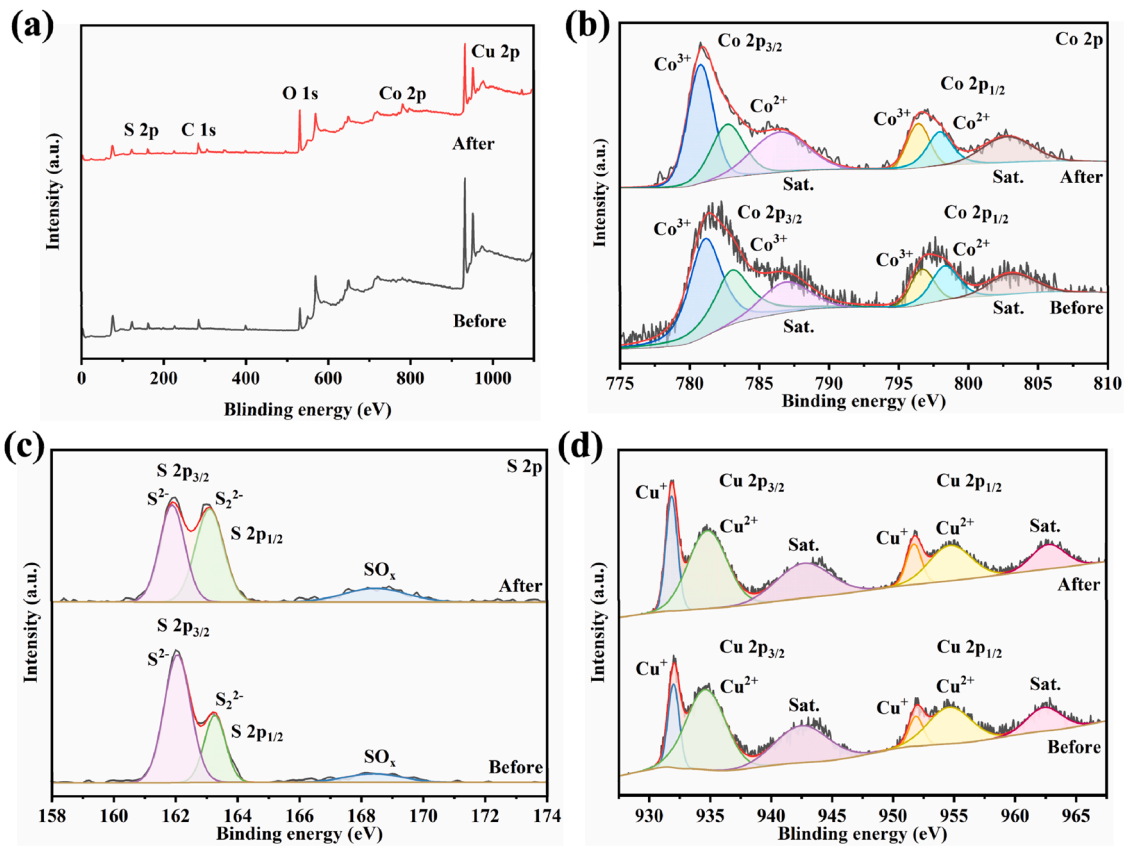

Fig. 7. (a) XPS survey spectra of CoS_x-CuS_x/CF. High-resolution XPS spectra of (b) Co 2p, (c) S 2p and (d) Cu 2p for CoS_x-CuS_x/CF.

decreased from 97.6% to 92.0% (0.1 mM $H_2PO_4^-$) and 80.5% (1.0 mM $H_2PO_4^-$) due to the adsorption of $H_2PO_4^-$ on the surface of CoS_x-CuS_x, inhibiting the exposure of active sites and SMX degradation (Chen et al., 2011).

$$Cl^- + HSO_5^- + H^+ \rightarrow SO_4^{2-} + Cl_2 + H_2 \quad (3)$$

$$Cl^- + SO_4^{\cdot-} \rightarrow SO_4^{2-} + Cl \quad (4)$$

$$Cl^- + \cdot OH \rightarrow OH^- + Cl \quad (5)$$

$$Cl^- + \cdot OH \rightarrow ClOH^- \quad (6)$$

$$ClOH^- + H^+ \rightarrow H_2O + Cl \quad (7)$$

$$Cl\cdot + Cl^- \rightarrow Cl_2^{\cdot-} \quad (8)$$

$$Cl_2^{\cdot-} + Cl_2^{\cdot-} \rightarrow Cl_2 + 2Cl^- \quad (9)$$

$$CO_3^{2-} + H_2O \rightleftharpoons HCO_3^- + OH^- \quad (10)$$

$$CO_3^{2-} + SO_4^{\cdot-} \rightarrow SO_4^{2-} + CO_3^{\cdot-} \quad (11)$$

$$CO_3^{2-} + \cdot OH \rightarrow OH^- + CO_3^{\cdot-} \quad (12)$$

$$NO_3^- + SO_4^{\cdot-} \rightarrow SO_4^{2-} + NO_3\cdot \quad (13)$$

$$NO_3^- + \cdot OH \rightarrow OH^- + NO_3\cdot \quad (14)$$

Natural organic matters (NOM) are important components in natural water, which usually inhibit the organic pollutants' degradation (Yang et al., 2019, Ramel et al., 2012). Humic acid (HA), as a typical NOM, was chosen to determine the effect on SMX degradation. As displayed in Fig. 5e, SMX degradation efficiency decreased from 97.6% to 90.9% (0.1 mM HA) and 82.2% (1.0 mM HA), which could be attributed to the competition between SMX and HA for ROS. The presence of HA sharply consumed the generated ROS (Xie et al., 2015), inhibiting the SMX degradation.

To further determine the potentially practical application of CoS_x-CuS_x/CF, the SMX degradation experiments in actual water bodies including lake water and tap water were conducted. As shown in the Fig. 5f, the SMX degradation efficiency decreased from 97.6% to 61.9% and 71.0% in lake water and tap water, respectively. The obvious inhibition would be ascribed to the effects of co-existing anions and natural organic matters in the actual water. It is worth noting that the SMX degradation efficiency became much better when the PMS dosage increased from 0.1 mM to 0.2 mM, which demonstrated that the inhibitory effect caused by coexisting species in actual water could be effectively solved by increasing PMS concentration.

3.5. The catalytic peroxymonosulfate activation mechanism

The ROS like $SO_4^{\cdot-}$,·OH, superoxide radical ($O_2^{\cdot-}$) and singlet oxygen ($^1O_2$) were always generated in the SR-AOPs (Giannakis et al., 2021; Huang et al., 2021b). In order to study the dominated active species for SMX degradation in CoS_x-CuS_x/CF-PMS system, the trapping experiments were carried out by adding different scavengers. It was reported that the reaction rate of EtOH with·OH (1.2–2.8 $\times 10^9$ M^{-1} s^{-1}) was similar to that with $SO_4^{\cdot-}$ (1.6–7.7 $\times 10^7$ M^{-1} s^{-1}), while tertiary butanol (TBA) reacted faster with·OH (3.8–7.6 $\times 10^8$ M^{-1} s^{-1}) than with $SO_4^{\cdot-}$ (4.0–9.1 $\times 10^5$ M^{-1} s^{-1}) (Zhao et al., 2021). Therefore, the TBA was selected to trap·OH, and EtOH was used to trap both·OH and $SO_4^{\cdot-}$ (Yi et al., 2021). As well, *p*-benzoquinone (BQ) and *β*-Carotene were chosen as the scavengers of $O_2^{\cdot-}$ and $^1O_2$, respectively (Ramel et al., 2012; Sun et al., 2019). It can be seen from Fig. 6a that SMX degradation efficiency rapidly decreased to 26.46%, 34.51%, 52.93% and 41.15% in the presence of EtOH, TBA, BQ and *β*-Carotene, respectively, suggesting that these four reactive species were involved in the SR-AOP process for SMX degradation. Furthermore, the ESR results (Fig. 6b–d) showed that no

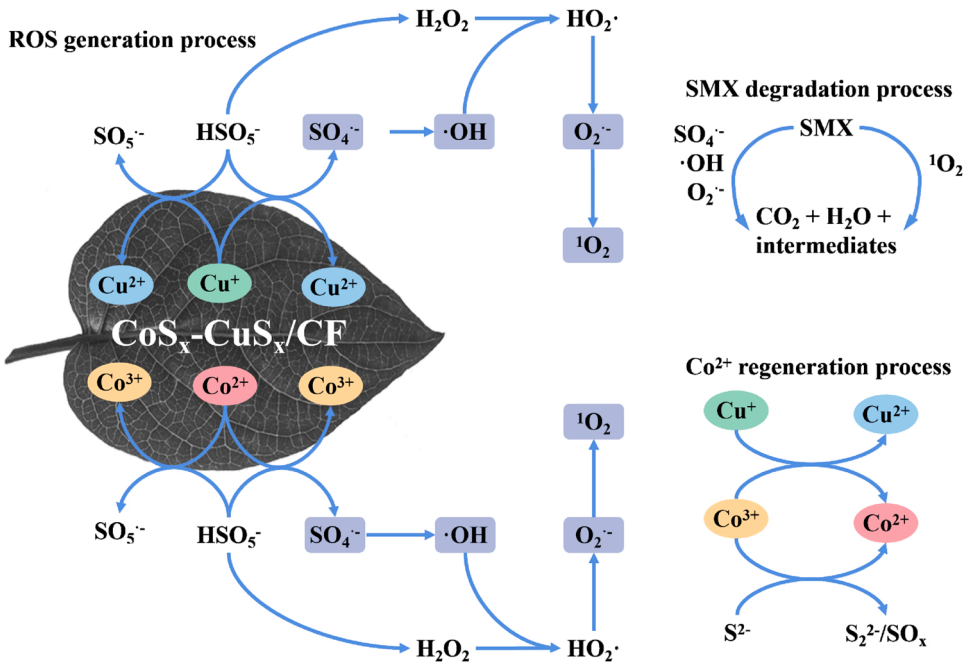

Fig. 8. The catalysis mechanism of SMX degradation over CoS_x-CuS_x/CF by PMS activation.

obvious signals related to ROS were observed in the individual CoS_x-CuS_x/CF or PMS system, while the typical peaks assigned to $SO_4^{·-}$,·OH, $O_2^{·-}$ and $^1O_2$ appeared in CoS_x-CuS_x/CF-PMS system, confirming the generation of these ROS through PMS activation over CoS_x-CuS_x/CF. The characteristic peaks of DMPO-$SO_4^{·-}$ were insignificantly compared with the DMPO-·OH, in which the·OH concentration (*ca.*723.87 μM) was much higher than $SO_4^{·-}$ (*ca.*18.49 μM) (Fig. S11). The above results revealed that·OH may be the main ROS, which was intrinsically different from the typical $SO_4^{·-}$-dominated system of Co-based/PMS (Li et al., 2020a, 2020b).

The surface microstructures and valence states of the elements in CoS_x-CuS_x/CF were confirmed by XPS analyses. As shown in Fig. 7a, the survey spectra proved the co-existence of Co, S, O, C, Cu elements in CoS_x-CuS_x/CF. In order to confirm the specific valence states of these elements, the high-resolution XPS spectra of Co 2p, S 2p and Cu 2p were measured, as shown in Fig. 7b–d. As for Co 2p XPS spectra, the characteristic peaks of Co $2p_{3/2}$ and Co $2p_{1/2}$ at about 783.1 and 798.3 eV could be ascribed to Co^{2+}, while the peaks at about 781.1 and 796.4 eV were assigned to Co^{3+} (Chauhan et al., 2017). The content of Co^{2+} increased (from 20.7% to 22.9%) while Co^{3+} decreased (from 27.1% to 25.6%) after SMX degradation, revealing that the reduction reaction between Co^{3+} and Co^{2+} occurred during the PMS activation process. The S 2p XPS spectra could be fitted by three peaks at 162.1, 163.5 and 169.0 eV, belonging to the S^{2-}, S_2^{2-} and SO_x, respectively (Ma et al., 2018; Li et al., 2020a, 2020b). It was observed that the amount of S^{2-} decreased (from 63.7% to 41.5%) while S_2^{2-} (from 27.0% to 44.6%) and SO_x (from 9.3% to 13.9%) increased after SMX degradation, suggesting that partial S^{2-} was oxidized into S_2^{2-} and SO_x. It can be reasonably speculated from the above discussion that the highly reductive sulfur species on the surface of CoS_x-CuS_x/CF facilitated the regeneration of

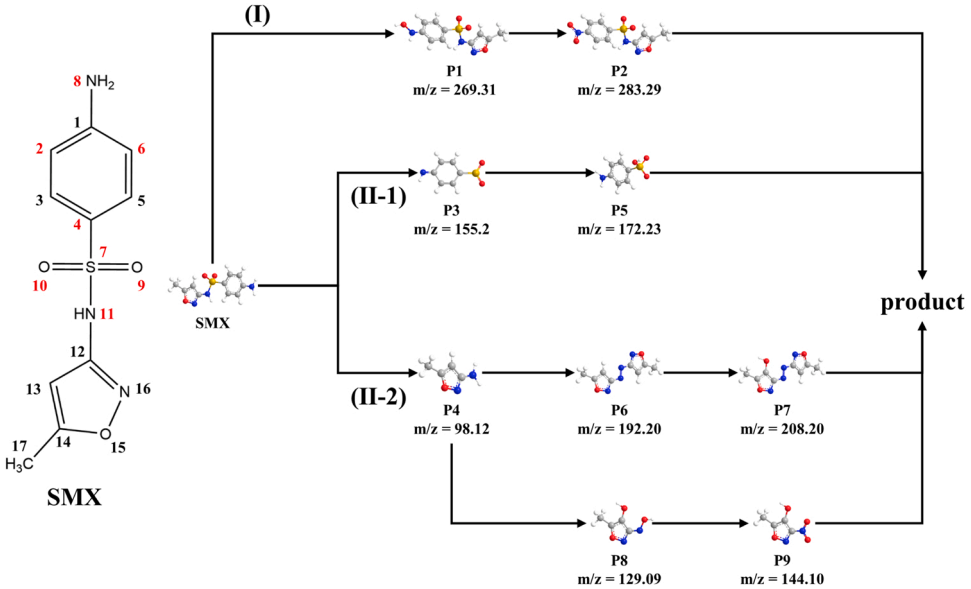

Fig. 9. The proposed SMX degradation pathways by catalytic SR-AOPs process over CoS_x-CuS_x/CF.

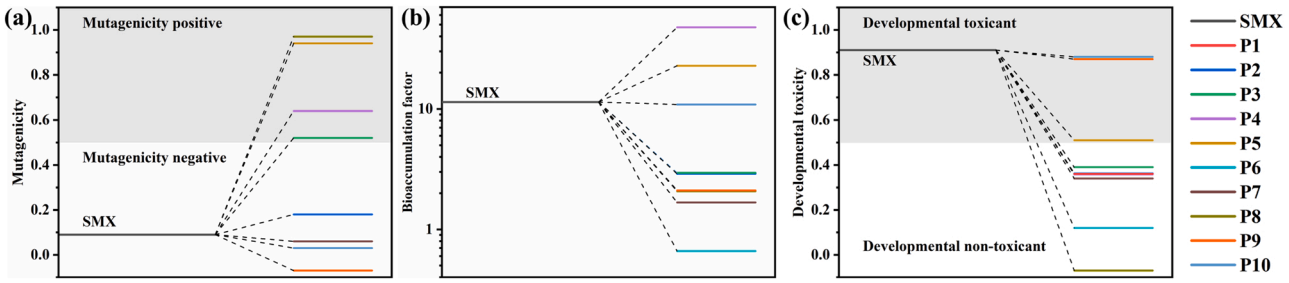

Fig. 10. (a) Bioaccumulation factor, (b) Mutagenicity and (c) Developmental toxicity of SMX and the degradation intermediates.

Co^{2+}, which was beneficial to the activation of PMS and the degradation of SMX. As well, the amount of Cu^{+} decreased (from 21.4% to 15.4%) while Cu^{2+} increased (from 49.4% to 53.4%) after SMX degradation, implying that some Cu^{+} would be oxidized by Co^{3+} into Cu^{2+}. Meanwhile, the PMS activation by Cu^{+} could also generate Cu^{2+} (Wang et al., 2020). Fig. S7 showed that the SMX degradation efficiency in CuS_x/CF-PMS system was better than that in individual PMS system, indicating that Cu species were also involved in the PMS activation process.

Based on the above analyses, the possible reaction mechanism was proposed (Fig. 8). First of all, PMS was activated by the superficial Co^{2+} and Cu^{+} sites of CoS_x-CuS_x/CF to generate $SO_4^{\cdot-}$ (Eq. 13). Meanwhile, the Co^{2+} and Cu^{+} could be regenerated by PMS (Eq. 14), which was frankly very slow process. The generated $SO_4^{\cdot-}$ would react with water molecules to produce ·OH and $O_2^{\cdot-}$ (Eqs. 15–18) (Qi et al., 2016), and then some $O_2^{\cdot-}$ would react with water to produce $^1O_2$ (Eq. 19) (Zeng et al., 2020). The generated $SO_4^{\cdot-}$, ·OH and $O_2^{\cdot-}$ and $^1O_2$ could degrade SMX (Eq. 20) into different intermediates or even CO_2 and H_2O. The S^{2-}, as an electron donor, was able to reduce Co^{3+} and Cu^{2+} into Co^{2+} and Cu^{+}, respectively (Eq. 21) (Ai et al., 2015; Qi et al., 2016; Zeng et al., 2020; Peng et al., 2020), which was beneficial to the PMS activation and SMX degradation. Moreover, the formation of the heterojunction between CuS_x and CoS_x facilitated the electron transfer from Cu^{+} to Co^{3+} (Eq. 22), realizing the rapid regeneration of Co^{2+}, which tremendously promoted the catalytic activity for PMS activation and SMX degradation.

$$Co^{2+}/Cu^{+} + HSO_5^{-} \rightarrow Co^{3+}/Cu^{2+} + SO_4^{\cdot-} + HO^{-} \quad (13')$$

$$Co^{3+}/Cu^{2+} + HSO_5^{-} \rightarrow Co^{2+}/Cu^{+} + SO_5^{\cdot-} + H^{+} \quad (14')$$

$$SO_4^{\cdot-} + HO^{-}/H_2O \rightarrow SO_4^{2-} + \cdot OH \quad (15)$$

$$HSO_5^{-} + H_2O \rightarrow H_2O_2 + HSO_4^{-} \quad (16)$$

$$\cdot OH + H_2O_2 \rightarrow HO_2^{\cdot-} \quad (17)$$

$$HO_2^{\cdot-} \rightarrow H^{+} + O_2^{\cdot-} \quad (18)$$

$$O_2^{\cdot-} + 2H_2O \rightarrow {}^1O_2 + H_2O_2 + HO^{-} \quad (19)$$

$$SO_4^{\cdot-}/O_2^{\cdot-}/\cdot OH/{}^1O_2 + SMX \rightarrow CO_2 + H_2O + \text{intermediates} \quad (20)$$

$$Co^{3+}/Cu^{2+} + S_2^{-} \rightarrow Co^{2+}/Cu^{+} + S_2^{2-}/SO_x \quad (21)$$

$$Co^{3+} + Cu^{+} \rightarrow Co^{2+} + Cu^{2+} \quad (22)$$

3.6. SMX degradation pathways and toxicity analysis

Fukui function (f_k^0) was generally employed to determine the most

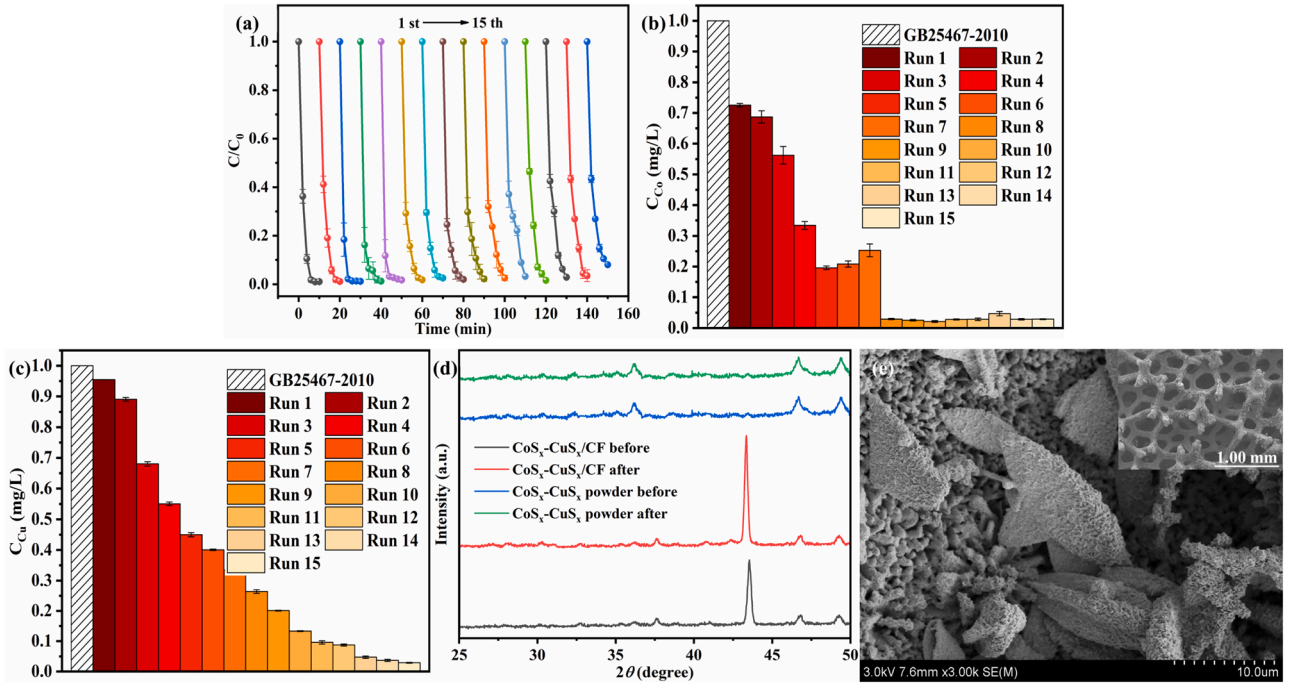

Fig. 11. (a) Reusability of CoS_x-CuS_x/CF for the removal of SMX; (b) Co and (c) Cu leaching concentrations after each cycle in CoS_x-CuS_x/CF-PMS system; (d) XRD patterns of CoS_x-CuS_x/CF and CoS_x-CuS_x before and after catalytic reaction; (e) SEM images of CoS_x-CuS_x/CF after reaction. ($[SMX]_0$ = 5 mg/L, initial pH = 9.0, $[PMS]_0$ = 0.1 mM, $[CoS_x\text{-}CuS_x]_0$ = 90 mg/L).

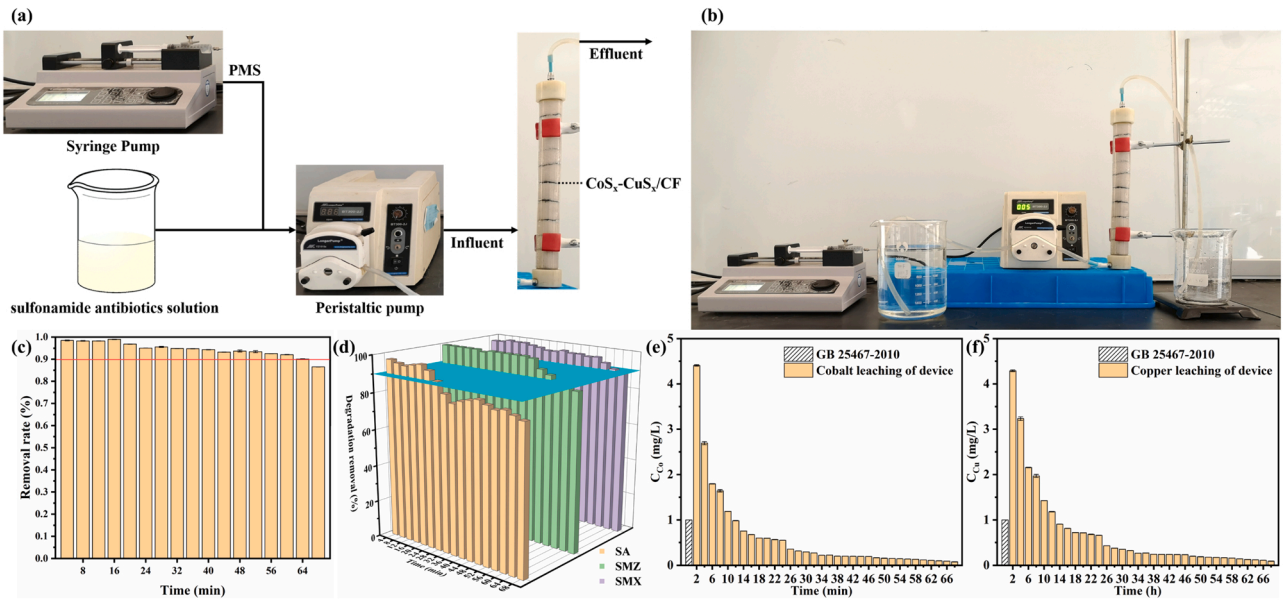

Fig. 12. (a) The sketch illustration and (b) photograph of the self-developed device for continuous-flow fixed-bed operation; (c) SMX degradation efficiencies over CoS_x-CuS_x/CF using the device in the individual SMX solution; (d) Degradation efficiencies of sulfonamide antibiotics using the device in a mixed solution containing three sulfonamides antibiotics; (e) Co and (f) Cu leaching concentrations after catalytic reactions.

vulnerable sites of SMX in the presence of radicals. Guo et al. have calculated the vulnerable sites of SMX in the presence of free radicals by the Fukui function calculations. As shown in Fig. 9, C2, C4, C6, S7, N8, O9, O10 and N11 of SMX were the most favorable sites for free radical attack (Du et al., 2017). Besides, based on the UHPLC-MS intermediate identification, two feasible pathways for SMX degradation via the aniline ring oxidation (pathway I) and S-N bond cleavage (pathway II) were proposed (Fig. 9) (Guo et al., 2020a, 2020b; Bao et al., 2019; Li et al., 2019; Xu et al., 2019). In pathway I, the -NH_2 group was firstly attacked by ROS to form a hydroxylamine derivative (P1) that can be further oxidized into a nitro derivative (P2). In pathway II, the S-N bond would be easily attacked by ROS to form P3 and P4, in which P3 can be further oxidized into P5. Besides, P6 was formed from P4 via the coupling reaction of -NH_2 group, and then P6 would be further oxidized by·OH into P7 by hydroxylation. Moreover, P4 might be oxidized by $^1O_2$ into P8 and P9. Considered that the TOC removal was 61.0%, the intermediates would be finally mineralized into H_2O and CO_2, NH_4^+ and NO_3^- (Bensalah et al., 2020; Midassi et al., 2020).

The toxicity of the intermediates during the degradation process is another significant indicator to evaluate catalysts (Yin et al., 2020). The bioaccumulation factor, mutagenicity and developmental toxicity of SMX and the intermediates were evaluated by the Toxicity Estimation Software (T.E.S.T.). As shown in Fig. 10, although part of the intermediates for bioaccumulation factor increased, most of them for mutagenicity and developmental toxicity declined. Taking into consideration the high TOC removal (61.0%), we believed that the CoS_x-CuS_x/CF would be a potential candidate for actual wastewater treatment.

3.7. Reusability of CoS_x-CuS_x/CF for the SMX degradation

The reusability is an important factor to evaluate catalysts and determine the possibility of practical application (Zhang et al., 2021; Sun et al., 2019). As shown in Fig. 11a, no obvious decrease of SMX degradation efficiency of CoS_x-CuS_x/CF was observed even after 15 cycles. Fig. 11b–c showed that the leaching Co and Cu concentrations after each cycle are lower than the specified value (< 1.0 mg/L) in the standard (emission standard of industrial pollutants for copper, nickel, cobalt (GB 25467-2010)). The morphology and structure of CoS_x-CuS_x/CF were not changed obviously even after 15 cycles of catalytic experiments (Fig. 11d–e), revealing its good stability and reusability.

3.8. The application of the self-developed fixed-bed reactor

In order to verify the possibility in practical application of CoS_x-CuS_x/CF, a self-developed fixed-bed reactor was constructed, in which CoS_x-CuS_x/CF and silica sand were packed successively in a polymethyl methacrylate tube (Figs. 12a-10b). The velocities of the SMX and PMS flows were controlled by peristaltic pump and syringe pump, respectively. As shown in Fig. 12c, the long-term continuous and efficient catalytic activation of PMS for sulfonamide antibiotics degradation was achieved, in which no obvious decrease of degradation efficiency was observed even up to 64 h. To further prove the excellent performance of CoS_x-CuS_x/CF, a aqueous solution containing the matrix of SMX (1.5 mg/L), SA (1.5 mg/L) and SMZ (1.5 mg/L) was adopted as simulated wastewater. It was found that more than 90% degradation efficiencies of these three sulfonamide antibiotics were achieved even after running for 28 h (Fig. 12d), in which the leaching Co and Cu concentrations gradually decreased below the standard value (emission standard of industrial pollutants for copper, nickel, cobalt (GB 25467-2010)) (Fig. 12e–f). It can be calculated that the handling capacity of the device for wastewater reached 1.5 L/h, which can be further optimized by tuning CoS_x-CuS_x/CF dosage and rotate speed of peristaltic pump, displaying potential application in industrial wastewater treatment.

4. Conclusion

Considering the good reusability of supported materials, the CoS_x-CuS_x/CF were successfully prepared via solvothermal method, in which the introduction of CF substrate contributed to the synergistic effect of CoS_x and CuS_x. The CoS_x-CuS_x/CF were demonstrated as a more efficient activator of SR-AOP for the PMS activation without light. Under the optimal conditions, the CoS_x-CuS_x/CF could degrade 97.0% of SMX within 10 min. The Cu^+ and reductive S species promoted the Co^{2+} regeneration that was crucial to the SMX degradation. It was found that the co-existing anions and the NOM exerted negative influences on the SR-AOP activation. As for real water, the above negative influences

could be overcome by increasing the PMS dosage. The ROS including radical species ($SO_4^{\cdot-}$,·OH and $O_2^{\cdot-}$) and non-radical species ($^1O_2$) could be responsible for the superior SMX degradation performance. The self-developed fixed-bed reactor was designed and used for long-term continuous and efficient wastewater treatment, which provided a new feasible way to remove antibiotics via SR-AOP activation over heterogeneous CoS_x-based supported catalysts.

CRediT authorship contribution statement

Aofei Du: Data curation, Investigation, Visualization, Software, Writing – original draft preparation. **Huifen Fu:** Conceptualization, Methodology, Supervision, Writing – review & editing. **Peng Wang:** Resources, Instrumental. **Chen Zhao:** Software, Methodology. **Chong-Chen Wang:** Funding acquisition, Supervision, Project administration, Writing – review & editing.

Declaration of Competing Interest

The authors declare that they have no known competing financial interests or personal relationships that could have appeared to influence the work reported in this paper.

Acknowledgments

This work was supported by National Natural Science Foundation of China, China (21806008, 22176012, 21876008), Beijing Natural Science Foundation, China (8202016), Great Wall Scholars Training Program Project of Beijing Municipality Universities, China (CIT&TCD20180323), Beijing Talent Project, China (2020A27), Science and Technology General Project of Beijing Municipal Education Commission, China (KM202110016010) and The Fundamental Research Funds for Beijing University of Civil Engineering and Architecture, China (X20147/X20141/X20135/X20146).

Appendix A. Supporting information

Supplementary data associated with this article can be found in the online version at doi:10.1016/j.jhazmat.2021.128134.

References

Ai, G., Mo, R., Li, H., Zhong, J., 2015. Cobalt phosphate modified TiO_2 nanowire arrays as co-catalysts for solar water splitting. Nanoscale 7, 6722–6728.
Ao, X., Liu, W., 2017. Degradation of sulfamethoxazole by medium pressure UV and oxidants: Peroxymonosulfate, persulfate, and hydrogen peroxide. Chem. Eng. J. 313, 629–637.
Bao, Y., Oh, W., Da, Lim, T.T., Wang, R., Webster, R.D., Hu, X., 2019. Elucidation of stoichiometric efficiency, radical generation and transformation pathway during catalytic oxidation of sulfamethoxazole via peroxymonosulfate activation. Water Res. 151, 64–74.
Bensalah, N., Midassi, S., Ahmad, M.I., Bedoui, A., 2020. Degradation of hydroxychloroquine by electrochemical advanced oxidation processes. Chem. Eng. J. 402, 126279.
Cai, P., Liu, T., Zhang, L., Cheng, B., Yu, J., 2020. ZIF-67 derived nickel cobalt sulfide hollow cages for high-performance supercapacitors. Appl. Surf. Sci. 504, 144501.
Cao, J., Lai, L., Lai, B., Yao, G., Chen, X., Song, L., 2019. Degradation of tetracycline by peroxymonosulfate activated with zero-valent iron: performance, intermediates, toxicity and mechanism. Chem. Eng. J. 364, 45–56.
Chauhan, M., Reddy, K.P., Gopinath, C.S., Deka, S., 2017. Copper cobalt sulfide nanosheets realizing a promising electrocatalytic oxygen evolution reaction. ACS Catal. 7, 5871–5879.
Chen, C.Y., Shih, Z.Y., Yang, Z., Chang, H.T., 2012. Carbon nanotubes/cobalt sulfide composites as potential high-rate and high-efficiency supercapacitors. J. Power Sources 215, 43–47.
Chen, G., Yu, Y., Liang, L., Duan, X., Li, R., Lu, X., Yan, B., Li, N., Wang, S., 2021a. Remediation of antibiotic wastewater by coupled photocatalytic and persulfate oxidation system: a critical review. J. Hazard. Mater. 408, 124461.
Chen, H., Luo, H., Lan, Y., Dong, T., Hu, B., Wang, Y., 2011. Removal of tetracycline from aqueous solutions using polyvinylpyrrolidone (PVP-K30) modified nanoscale zero valent iron. J. Hazard. Mater. 192, 44–53.
Chen, J., Zhang, L., Huang, T., Li, W., Wang, Y., Wang, Z., 2016. Decolorization of azo dye by peroxymonosulfate activated by carbon nanotube: radical versus non-radical mechanism. J. Hazard. Mater. 320, 571–580.
Chen, M., Wang, N., Wang, X., Zhou, Y., Zhu, L., 2021b. Enhanced degradation of tetrabromobisphenol A by magnetic Fe_3O_4@ZIF-67 composites as a heterogeneous Fenton-like catalyst. Chem. Eng. J. 413, 127539.
Chen, Y., Duan, X., Zhou, X., Wang, R., Wang, S., Ren, N., Ho, S.H., 2021c. Advanced oxidation processes for water disinfection: Features, mechanisms and prospects. Chem. Eng. J. 409, 128207.
Du, J., Guo, W., Wang, H., Yin, R., Zheng, H., Feng, X., Che, D., Ren, N., 2017. Hydroxyl radical dominated degradation of aquatic sulfamethoxazole by Fe^0/bisulfite/O_2: kinetics, mechanisms, and pathways Juanshan. Water Res. 138, 323–332.
Fang, X., Gan, L., Wang, L., Gong, H., Xu, L., Wu, Y., Lu, H., Han, S., Cui, J., Xia, C., 2021. Enhanced degradation of bisphenol A by mixed ZIF derived CoZn oxide encapsulated N-doped carbon via peroxymonosulfate activation: the importance of N doping amount. J. Hazard. Mater. 419, 126363.
Fu, H., Wang, C.-C., Liu, W., 2021. MOFs for water purification. Chin. Chem. Lett. https://doi.org/10.1016/j.cclet.2021.08.065.
Giannakis, S., Lin, K.Y.A., Ghanbari, F., 2021. A review of the recent advances on the treatment of industrial wastewaters by sulfate radical-based advanced oxidation processes (SR-AOPs). Chem. Eng. J. 406, 127083.
Govindan, K., Raja, M., Noel, M., James, E.J., 2014. Degradation of pentachlorophenol by hydroxyl radicals and sulfate radicals using electrochemical activation of peroxomonosulfate, peroxodisulfate and hydrogen peroxide. J. Hazard. Mater. 272, 42–51.
Guan, Y.H., Ma, J., Li, X.C., Fang, J.Y., Chen, L.W., 2011. Influence of pH on the formation of sulfate and hydroxyl radicals in the UV/Peroxymonosulfate system. Environ. Sci. Technol. 45, 9308–9314.
Guo, R., Nengzi, L., Chen, Y., Li, Y., Zhang, X., Cheng, X., 2020a. Efficient degradation of sulfamethoxazole by CuCo LDH and LDH@fibers composite membrane activating peroxymonosulfate. Chem. Eng. J. 398, 125676.
Guo, R., Wang, Y., Li, J., Cheng, X., Dionysiou, D.D., 2020b. Sulfamethoxazole degradation by visible light assisted peroxymonosulfate process based on nanohybrid manganese dioxide incorporating ferric oxide. Appl. Catal. B Environ. 278, 119297.
Gupta, D.K., Neupane, S., Yadav, H.C., Subedi, V., Singh, S., Yadav, R.J., Das, A.K., Yadav, B., Nakarmi, K.B., Karki, N., Yadav, A.P., 2021. Trace level monitoring of Cu (II) ion using CuS particles based membrane electrochemical sensor. Heliyon 7, 2–8.
He, Y., Zhang, X., Wang, S., Meng, J., Sui, Y., Wei, F., Qi, J., Meng, Q., Ren, Y., Zhuang, D., 2020. Rubik's cube-like Ni_3S_4/CuS_2 nanocomposite for high-performance supercapacitors. J. Alloy. Compd. 847, 156312.
Huang, C., Zhang, H., Zheng, K., Zhang, Z., Jiang, Q., Li, J., 2021a. Two-dimensional hydrophilic ZIF-L as a highly-selective adsorbent for rapid phosphate removal from wastewater. Sci. Total Environ. 785, 147382.
Huang, D., Zhang, G., Yi, J., Cheng, M., Lai, C., Xu, P., Zhang, C., Liu, Y., Zhou, C., Xue, W., Wang, R., Li, Z., Chen, S., 2021b. Progress and challenges of metal-organic frameworks-based materials for SR-AOPs applications in water treatment. Chemosphere 263, 127672.
Huang, Y.H., Huang, Y.F., Huang, C., Chen, C.Y., 2009. Efficient decolorization of azo dye reactive black B involving aromatic fragment degradation in buffered Co^{2+}/PMS oxidative processes with a ppb level dosage of Co^{2+}-catalyst. J. Hazard. Mater. 170, 1110–1118.
Ji, K., Matras-Postolek, K., Shi, R., Chen, L., Che, Q., Wang, J., Yue, Y., Yang, P., 2022. MoS_2/CoS_2 heterostructures embedded in N-doped carbon nanosheets towards enhanced hydrogen evolution reaction. J. Alloy. Compd. 891, 161962.
Li, W., Li, S., Tang, Y., Yang, X., Zhang, W., Zhang, X., Chai, H., Huang, Y., 2020a. Highly efficient activation of peroxymonosulfate by cobalt sulfide hollow nanospheres for fast ciprofloxacin degradation. J. Hazard. Mater. 389, 121856.
Li, Y., Li, J., Pan, Y., Xiong, Z., Yao, G., Xie, R., Lai, B., 2020b. Peroxymonosulfate activation on $FeCo_2S_4$ modified g-C_3N_4 ($FeCo_2S_4$-CN): mechanism of singlet oxygen evolution for nonradical efficient degradation of sulfamethoxazole. Chem. Eng. J. 384, 123361.
Li, Y., Liu, S., Chen, W., Li, S., Shi, L., Zhao, Y., 2017. Facile synthesis of flower-like cobalt sulfide hierarchitectures with superior electrode performance for supercapacitors. J. Alloy. Compd. 712, 139–146.
Li, Y., Zhao, X., Yan, Y., Yan, J., Pan, Y., Zhang, Y., Lai, B., 2019. Enhanced sulfamethoxazole degradation by peroxymonosulfate activation with sulfide-modified microscale zero-valent iron (S-mFe^0): performance, mechanisms, and the role of sulfur species. Chem. Eng. J., 121302
Liu, G., Jiang, Z., Cao, K., Nair, S., Cheng, X., Zhao, J., Gomaa, H., Wu, H., Pan, F., 2017. Pervaporation performance comparison of hybrid membranes filled with two-dimensional ZIF-L nanosheets and zero-dimensional ZIF-8 nanoparticles. J. Memb. Sci. 523, 185–196.
Ma, W., Wang, N., Fan, Y., Tong, T., Han, X., Du, Y., 2018. Non-radical-dominated catalytic degradation of bisphenol A by ZIF-67 derived nitrogen-doped carbon nanotubes frameworks in the presence of peroxymonosulfate. Chem. Eng. J. 336, 721–731.
Midassi, S., Bedoui, A., Bensalah, N., 2020. Efficient degradation of chloroquine drug by electro-Fenton oxidation: Effects of operating conditions and degradation mechanism. Chemosphere 260, 127558.
Neta, P., Huie, R.E., Ross, A.B., 1988. Rate constants for reactions of inorganic radicals in aqueous solution. J. Phys. Chem. Ref. Data 17, 1027–1284.
Oh, W.Da, Dong, Z., Ronn, G., Lim, T.T., 2017. Surface–active bismuth ferrite as superior peroxymonosulfate activator for aqueous sulfamethoxazole removal: performance, mechanism and quantification of sulfate radical. J. Hazard. Mater. 325, 71–81.

Peng, H., Cao, J., Xiong, W., Yang, Z., Jia, M., Sun, S., Xu, Z., Zhang, Y., Cai, H., 2021a. Two-dimension N-doped nanoporous carbon from KCl thermal exfoliation of Zn-ZIF-L: efficient adsorption for tetracycline and optimizing of response surface model. J. Hazard. Mater. 402, 123498.

Peng, H., Xiong, W., Yang, Z., Cao, J., Jia, M., Xiang, Y., Hu, Q., Xu, Z., 2021b. Facile fabrication of three-dimensional hierarchical porous ZIF-L/gelatin aerogel: highly efficient adsorbent with excellent recyclability towards antibiotics. Chem. Eng. J. 426, 130798.

Peng, J., Zhou, H., Liu, W., Ao, Z., Ji, H., Liu, Y., Su, S., Yao, G., Lai, B., 2020. Insights into heterogeneous catalytic activation of peroxymonosulfate by natural chalcopyrite: pH-dependent radical generation, degradation pathway and mechanism. Chem. Eng. J. 397, 125387.

Qi, C., Liu, X., Ma, J., Lin, C., Li, X., Zhang, H., 2016. Activation of peroxymonosulfate by base: implications for the degradation of organic pollutants. Chemosphere 151, 280–288.

Qi, F., Chu, W., Xu, B., 2014. Modeling the heterogeneous peroxymonosulfate/Co-MCM41 process for the degradation of caffeine and the study of influence of cobalt sources. Chem. Eng. J. 235, 10–18.

Ramel, F., Birtic, S., Cuiné, S., Triantaphylidès, C., Ravanat, J.L., Havaux, M., 2012. Chemical quenching of singlet oxygen by carotenoids in plants. Plant Physiol. 158, 1267–1278.

Ren, W., Zhou, P., Nie, G., Cheng, C., Duan, X., Zhang, H., Wang, S., 2020. Hydroxyl radical dominated elimination of plasticizers by peroxymonosulfate on metal-free boron: kinetics and mechanisms. Water Res. 186, 116361.

Sun, P., Liu, H., Feng, M., Guo, L., Zhai, Z., Fang, Y., Zhang, X., Sharma, V.K., 2019. Nitrogen-sulfur co-doped industrial graphene as an efficient peroxymonosulfate activator: singlet oxygen-dominated catalytic degradation of organic contaminants. Appl. Catal. B Environ. 251, 335–345.

Tai, C., Peng, J.F., Liu, J.F., Jiang, G., Bin, Zou, H., 2004. Determination of hydroxyl radicals in advanced oxidation processes with dimethyl sulfoxide trapping and liquid chromatography. Anal. Chim. Acta 527, 73–80.

Wang, F., Fu, H., Wang, F.-X., Zhang, X.-W., Wang, P., Zhao, C., Wang, C.-C., 2022. Enhanced catalytic sulfamethoxazole degradation via peroxymonosulfate activation over amorphous CoS_x@SiO_2 nanocages derived from ZIF-67. J. Hazard. Mater. 423, 126998.

Wang, S., Wang, J., 2020. Peroxymonosulfate activation by Co_9S_8@ S and N co-doped biochar for sulfamethoxazole degradation. Chem. Eng. J. 385, 123933.

Wang, X., Ding, Y., Dionysiou, D.D., Liu, C., Tong, Y., Gao, J., Fang, G., Zhou, D., 2020. Efficient activation of peroxymonosulfate by copper sulfide for diethyl phthalate degradation: performance, radical generation and mechanism. Sci. Total Environ. 749, 142387.

Wang, Z., Ai, L., Huang, Y., Zhang, J., Li, S., Chen, J., Yang, F., 2017. Degradation of azo dye with activated peroxygens: When zero-valent iron meets chloride. RSC Adv. 7, 30941–30948.

Wu, L., Wang, C.C., Chu, H.Y., Yi, X.H., Wang, P., Zhao, C., Fu, H., 2021. Bisphenol A cleanup over MIL-100(Fe)/CoS composites: pivotal role of Fe-S bond in regenerating Fe^{2+} ions for boosted degradation performance. Chemosphere 280, 130659.

Wu, X., Zhao, W., Huang, Y., Zhang, G., 2020. A mechanistic study of amorphous CoS_x cages as advanced oxidation catalysts for excellent peroxymonosulfate activation towards antibiotics degradation. Chem. Eng. J. 381, 122768.

Xie, P., Ma, J., Liu, W., Zou, J., Yue, S., Li, X., Wiesner, M.R., Fang, J., 2015. Removal of 2-MIB and geosmin using UV/persulfate: contributions of hydroxyl and sulfate radicals. Water Res. 69, 223–233.

Xu, M., Li, J., Yan, Y., Zhao, X., Yan, J., Zhang, Y., Lai, B., Chen, X., Song, L., 2019. Catalytic degradation of sulfamethoxazole through peroxymonosulfate activated with expanded graphite loaded $CoFe_2O_4$ particles. Chem. Eng. J. 369, 403–413.

Yan, J., Li, J., Peng, J., Zhang, H., Zhang, Y., Lai, B., 2019. Efficient degradation of sulfamethoxazole by the CuO@Al_2O_3 (EPC) coupled PMS system: optimization, degradation pathways and toxicity evaluation. Chem. Eng. J. 359, 1097–1110.

Yang, Q., Ma, Y., Chen, F., Yao, F., Sun, J., Wang, S., Yi, K., Hou, L., Li, X., Wang, D., 2019. Recent advances in photo-activated sulfate radical-advanced oxidation process (SR-AOP) for refractory organic pollutants removal in water. Chem. Eng. J. 378, 122149.

Yang, Z., Chen, C.Y., Chang, H.T., 2011. Supercapacitors incorporating hollow cobalt sulfide hexagonal nanosheets. J. Power Sources 196, 7874–7877.

Ye, J., Li, C., Yan, Y., 2020. Core-shell ZIF-67/ZIF-8-derived sea urchin-like cobalt/nitrogen Co-doped carbon nanotube hollow frameworks for ultrahigh adsorption and catalytic activities. J. Taiwan Inst. Chem. Eng. 112, 202–211.

Yi, X.H., Ji, H., Wang, C.C., Li, Y., Li, Y.H., Zhao, C., Wang, A., Fu, H., Wang, P., Zhao, X., Liu, W., 2021. Photocatalysis-activated SR-AOP over PDINH/MIL-88A(Fe) composites for boosted chloroquine phosphate degradation: performance, mechanism, pathway and DFT calculations. Appl. Catal. B Environ. 293, 120229.

Yin, R., Chen, Y., He, S., Li, W., Zeng, L., Guo, W., Zhu, M., 2020. In situ photoreduction of structural Fe(III) in a metal–organic framework for peroxydisulfate activation and efficient removal of antibiotics in real wastewater. J. Hazard. Mater. 388, 121996.

Yu, B., Ji, Y., Hu, X., Liu, Y., Yuan, J., Lei, S., Zhong, G., Weng, Z., Zhan, H., Wen, Z., 2022. Heterostructured Cu_2S@ZnS/C composite with fast interfacial reaction kinetics for high-performance 3D-printed Sodium-Ion batteries. Chem. Eng. J. 430, 132993.

Yu, D., Wu, B., Ge, L., Wu, L., Wang, H., Xu, T., 2016. Decorating nanoporous ZIF-67-derived $NiCo_2O_4$ shells on a Co_3O_4 nanowire array core for battery-type electrodes with enhanced energy storage performance. J. Mater. Chem. A 4, 10878–10884.

Yu, J., Cui, Z., Li, X., Chen, D., Ji, J., Zhang, Q., Sui, J., Yu, L., Dong, L., 2020. Facile fabrication of ZIF-derived graphene-based 2D Zn/Co oxide hybrid for high-performance supercapacitors. J. Energy Storage 27, 101165.

Zeng, H., Deng, L., Zhang, H., Zhou, C., Shi, Z., 2020. Development of oxygen vacancies enriched CoAl hydroxide@hydroxysulfide hollow flowers for peroxymonosulfate activation: a highly efficient singlet oxygen-dominated oxidation process for sulfamethoxazole degradation. J. Hazard. Mater. 400, 123297.

Zhang, X.-W., Wang, F., Wang, C.-C., Wang, P., Fu, H., Zhao, C., 2021. Photocatalysis activation of peroxodisulfate over the supported Fe_3O_4 catalyst derived from MIL-88A(Fe) for efficient tetracycline hydrochloride degradation. Chem. Eng. J. 426, 131927.

Zhao, C., Wang, J., Chen, X., Wang, Z., Ji, H., Chen, L., Liu, W., Wang, C.C., 2021. Bifunctional $Bi_{12}O_{17}Cl_2$/MIL-100(Fe) composites toward photocatalytic Cr(VI) sequestration and activation of persulfate for bisphenol A degradation. Sci. Total Environ. 752, 141901.

Zhou, T., Zou, X., Mao, J., Wu, X., 2016. Decomposition of sulfadiazine in a sonochemical Fe0-catalyzed persulfate system: parameters optimizing and interferences of wastewater matrix. Appl. Catal. B Environ. 185, 31–41.

Zhu, C., Liu, F., Ling, C., Jiang, H., Wu, H., Li, A., 2019. Growth of graphene-supported hollow cobalt sulfide nanocrystals via MOF-templated ligand exchange as surface-bound radical sinks for highly efficient bisphenol A degradation. Appl. Catal. B Environ. 242, 238–248.

Zhu, M.P., Yang, J.C.E., Duan, X., Zhang, D.D., Wang, S., Yuan, B., Fu, M.L., 2020. Interfacial $CoAl_2O_4$ from ZIF-67@γ-Al_2O_3 pellets toward catalytic activation of peroxymonosulfate for metronidazole removal. Chem. Eng. J. 397, 125339.